Journal of Computational Physics 281 (2015) 316–333

Contents lists available at ScienceDirect

Journal of Computational Physics

www.elsevier.com/locate/jcp

A parameter estimation framework for patient-specific hemodynamic computations

Lucian Itu [a,d,*], Puneet Sharma [b], Tiziano Passerini [b], Ali Kamen [b], Constantin Suciu [c,d], Dorin Comaniciu [b]

[a] Imaging and Computer Vision, Siemens SRL, Corporate Technology, B-dul Eroilor nr. 5, Brasov, 500007, Romania
[b] Imaging and Computer Vision, Siemens Corporation, Corporate Technology, 755 College Road East, Princeton, NJ 08540, USA
[c] Siemens SRL, Corporate Technology, B-dul Eroilor nr. 5, Brasov, 500007, Romania
[d] Transilvania University of Brasov, B-dul Eroilor nr. 29, 500036, Brasov, Romania

ARTICLE INFO

Article history:
Received 24 July 2013
Received in revised form 30 May 2014
Accepted 15 October 2014
Available online 22 October 2014

Keywords:
Parameter estimation
Model personalization
Geometrical multiscale model
Windkessel
Blood flow
Hemodynamics

ABSTRACT

We propose a fully automated parameter estimation framework for performing patient-specific hemodynamic computations in arterial models. To determine the personalized values of the windkessel models, which are used as part of the geometrical multiscale circulation model, a parameter estimation problem is formulated. Clinical measurements of pressure and/or flow-rate are imposed as constraints to formulate a nonlinear system of equations, whose fixed point solution is sought. A key feature of the proposed method is a warm-start to the optimization procedure, with better initial solution for the nonlinear system of equations, to reduce the number of iterations needed for the calibration of the geometrical multiscale models. To achieve these goals, the initial solution, computed with a lumped parameter model, is adapted before solving the parameter estimation problem for the geometrical multiscale circulation model: the resistance and the compliance of the circulation model are estimated and compensated.

The proposed framework is evaluated on a patient-specific aortic model, a full body arterial model, and multiple idealized anatomical models representing different arterial segments. For each case it leads to the best performance in terms of number of iterations required for the computational model to be in close agreement with the clinical measurements.

1. Introduction

Blood-flow computations, when used in conjunction with patient-specific anatomical models extracted from medical images, provide important insights into the structure and function of the cardiovascular system. In recent years, these techniques have been proposed for diagnosis, risk stratification, and surgical planning [1–4].

Different approaches have been proposed for specifying the outlet boundary conditions, ranging from pressure or flow rate profiles to lumped parameter models (0D models). For an accurate patient-specific computation, the role of physiologically sound boundary conditions is well appreciated in the literature. The effect of distal vasculature is modeled by outlet boundary conditions coupled with the computational domain (region of interest), resulting in a geometrical multiscale model. The boundary conditions are represented by lumped parameter models, which are designed to capture one

* Corresponding author at: Transilvania University of Brasov, B-dul Eroilor nr. 29, 500036, Brasov, Romania. Tel.: +40 741029888.
E-mail addresses: lucian.itu@unitbv.ro (L. Itu), sharma.puneet@siemens.com (P. Sharma), ali.kamen@siemens.com (A. Kamen), constantin.suciu@siemens.com (C. Suciu), dorin.comaniciu@siemens.com (D. Comaniciu).

http://dx.doi.org/10.1016/j.jcp.2014.10.034
0021-9991/

(or more) of the i) total resistance, ii) total compliance, and iii) the wave propagation and reflection effects in the distal vasculature. The most widely used lumped parameter model is the three-element windkessel model [5], which is characterized by its simplicity (only three parameters), and ability to capture two important characteristics of the distal circulation (compliance and resistance).

In a clinical scenario, the values of the windkessel model parameters are not available on a per-patient basis. Instead, multiple pressure or flow measurements are usually available for each patient. A clinically feasible and accurate flow computation should not only be in agreement with these measurements, but should also have means to model other hemodynamic states for the same patient. To achieve this, one has to estimate a set of personalized windkessel model parameters, while ensuring that the computations match the measured data.

Different calibration procedures for the outlet boundary conditions have been proposed. Olufsen et al. [6] proposed a calibration method for determining the dynamic cerebral blood flow response to sudden hypotension during posture change. Their experimental calibration procedure depends strongly on the patient-specific state, i.e. on the position of the patient.

A fully automatic optimization-based calibration method for the windkessel models was suggested [7], where the input was specified by non-invasively acquired systolic/diastolic pressures and, in some cases, additional flow data. The windkessel parameters were obtained by solving a system of nonlinear equations, formulated based on a set of objectives for the pressure and flow rate waveforms at various locations. A Broyden method was employed for solving the nonlinear system of equations. The initial parameters values were determined by a reduced-order model, composed of only the windkessel models of the geometrical multiscale model.

An adjoint based method for calibrating the windkessel parameters was proposed [8], where the Jacobian was computed without the use of finite-differences, and eliminated the risk of that the Broyden's method would not converge for initial guesses far away from the solution. Furthermore, a reduced-order model with resistance outlet boundary conditions was introduced [9], under which the terminal resistance values of the arterial model of the arm were adapted to obtain desired flow rate distribution between vascular territories.

A competitive alternative to the above mentioned optimization based methods is represented by filtering based methods. These methods were successfully used to estimate different aspects of fluid–structure interaction applications, like arterial wall stiffness [10], the surrounding tissue support [11], or windkessel parameters [12].

In the current study, we propose a parameter estimation method for personalizing hemodynamic computations. The proposed method is inspired by the approach introduced previously [7], and has been developed based on the following strategies: a warm-start of the optimization procedure with better initial solution, and a reduction in the number of iterations performed for the calibration of the geometrical multiscale models (for simplifying phrasing, we will refer to geometrical multiscale models simply as multiscale models). The first strategy allows us to minimize the risk of a possible failure of the optimization approach due to a bad initial guess [8] – a fairly common occurrence for pathologic cases. Moreover, we achieve a faster computation time for the overall estimation method by reducing the number of repetitive iterations on the same geometry.

The parameter estimation method automatically determines the windkessel parameters, in the multiscale circulation model, by solving a system of nonlinear equations. To obtain an initial guess, the equations are first solved for a lumped parameter model. The main characteristic of the proposed method is that, when switching from the lumped model to the multiscale model, the windkessel parameters are appropriately adapted to take into account the hemodynamic properties (resistance and compliance) of the multiscale model.

The paper is organized as follows. In Section 2, we first briefly review the three-element windkessel model and the calibration method introduced previously [7]. Next, we introduce the proposed parameter estimation method, together with the algorithms used for estimating and compensating the resistance and compliance of the highest order model. Section 3 presents detailed calibration results for six different computational setups, including a patient-specific aortic coarctation (CoA) case and a full body arterial model. Results are reported for four different approaches: the calibration method for windkessel parameters proposed previously, the parameter estimation method with resistance compensation and direct compliance compensation, the parameter estimation method with resistance compensation and analytical compliance compensation and the parameter estimation method with resistance compensation and numerical compliance compensation. A discussion on the methodology is presented in Section 4.

2. Methods

In this section, we describe an efficient optimization-based algorithm, which ensures that the personalized flow computations are in close agreement with the physiological measurements. In the present study, we use a 1D-0D reduced-order geometrical multiscale model as proof of concept. One-dimensional models have been shown to accurately predict time-varying flow rate and pressure wave forms [13]. Most of the one-dimensional models introduced in literature use elastic wall laws [14–17], but viscoelastic arterial wall models have also been applied [18,19]. Further, recent research activities have shown the growing interest in the one-dimensional blood flow model not only for the computation of a full body arterial model, but also for specific parts of the circulation in pathologic situations: the coronary circulation [20], the abdominal aorta [21,22], proximal part of the aorta [23], and the aortic valve [24]. The 1D model used in this study has been previously introduced in [20,23]. Time-varying flow rate profiles are used as inlet boundary condition, while three-element

windkessel models were coupled at the outlets of the highest order model. The 3-element windkessel model is represented by the following relationship between instantaneous flow and pressure:

$$\frac{dp}{dt} = R_p \frac{dq}{dt} - \frac{p}{R_d \cdot C} + \frac{q(R_p + R_d)}{R_d \cdot C}, \tag{1}$$

where p is the instantaneous pressure at the inlet of the windkessel model, q is the instantaneous flow rate, R_p and R_d are the proximal and distal resistance respectively, and C is the compliance.

Next, we briefly review the calibration method proposed previously and introduce the proposed parameter estimation method.

2.1. Calibration method for windkessel parameters

The calibration method automatically estimates the free parameters (windkessel parameters) to ensure that the computed pressure and flow-rate values minimize the objective function [7]. More specifically, the algorithm iteratively estimates the total resistance of the windkessel model, R_t, the proximal resistance ratio, ρ, and the time constant of the exponential pressure decay in the windkessel model at zero flow, τ:

$$R_t = R_p + R_d, \tag{2}$$

$$\rho = R_p / R_t, \tag{3}$$

$$\tau = R_d \cdot C. \tag{4}$$

Measured pressure and/or flow rate values are used as objectives of the calibration method. The parameter estimation problem is formulated as a solution to a system of nonlinear equations, with each equation representing the residual error between the computed and measured quantity of interest. To determine the values of all the residuals ($\boldsymbol{f}(\boldsymbol{x}_i)$), a computation with the parameter values $\boldsymbol{x}_i$ is required. Since the absolute values of the adapted parameters and of the residuals generally differ by orders of magnitude, for the calibration method both the parameter and the objective residuals have been scaled using typical values, as is described below.

The nonlinear system of equations is first solved for a 0D model, composed of the windkessel models used in the multiscale model. To find an initial solution for the 0D model, a grid of physiological parameter value sets is considered. The parameter value set leading to the smallest L_2 norm for the objective residual, is used as initial solution for a dogleg trust region method, which determines the solution $\boldsymbol{x}_0$ used during the subsequent steps.

Next, a fixed-point approach is used to compute a finite-difference Jacobian which is determined using the typical step sizes, and is consistent with the chosen typical values of the objective residuals. The components of the Jacobian approximations are computed as follows:

$$J_{ij} = \frac{1}{s_j^{typ}} \left[\boldsymbol{f}\left(\boldsymbol{x}_0 + \frac{1}{2} s_j^{typ} \boldsymbol{e}_j\right) - \boldsymbol{f}\left(\boldsymbol{x}_0 - \frac{1}{2} s_j^{typ} \boldsymbol{e}_j\right) \right] \cdot \boldsymbol{e}_i, \tag{5}$$

where $\boldsymbol{e}_i$ and $\boldsymbol{e}_j$ represent the unit vectors in the ith and jth direction respectively, and s_j^{typ} is the typical step size for parameter j, given by:

$$s_j^{typ} = 1 \Big/ \sqrt{\sum_{i=1}^{n_{eq}} \left(J_{ij} / f_i^{typ}\right)}, \tag{6}$$

where f_i^{typ} is the typical value of the objective residual f_i.

The process composed of Eqs. (5) and (6) is an iterative procedure which is terminated once the Euclidean norm of the difference of two consecutive Jacobians, normalized by the corresponding f_i^{typ} and s_j^{typ} values, is less than 10^{-6}.

Next, the multiscale model is set up and run, and the objective residuals are evaluated. For the first run with the multiscale model, the solution variables are initialized based on the results obtained with the 0D model. Each computation, with a given set of parameter values, is run until the L_2 norms of the normalized differences between the pressure and flow rate profiles at the current and the previous cardiac cycle are smaller than 10^{-5}.

If all objective residuals are smaller than the tolerance limit (taken here equal to $f_i^{typ}/10$), the calibration method is terminated. Otherwise, a quasi-Newton method is employed to update the parameter values. First the Jacobian matrix is updated: since the computation of a finite-difference Jacobian matrix with the multiscale model is expensive, the Jacobian determined with the fixed-point approach is updated at each iteration, using:

$$\boldsymbol{J}_{i+1} = \boldsymbol{J}_i + \frac{[\boldsymbol{f}(\boldsymbol{x}_{i+1}) - \boldsymbol{f}(\boldsymbol{x}_i) - \boldsymbol{J}_i \boldsymbol{s}_i](\boldsymbol{D}_s^2 \boldsymbol{s}_i)^T}{\boldsymbol{s}_i^T \boldsymbol{D}_s^2 \boldsymbol{s}_i}, \tag{7}$$

where $\boldsymbol{s}_i = \boldsymbol{x}_{i+1} - \boldsymbol{x}_i$ is the current step and $\boldsymbol{D}_s$ is a diagonal scaling matrix:

$$(D_s)_{ij} = \begin{cases} 1/s_j^{typ}, & i = j \\ 0, & i \neq j \end{cases} \tag{8}$$

Finally, the new parameter values are estimated:

$$\boldsymbol{x}_{i+1} = \boldsymbol{x}_i - \boldsymbol{J}_i^{-1} \boldsymbol{f}(\boldsymbol{x}_i). \tag{9}$$

The main drawback of the above described calibration method is that the hemodynamic properties of the highest order model of the multiscale model are not taken into account when switching from the 0D model to the multiscale model. This aspect has several consequences. First of all, the solution obtained for the 0D model, which is used as initial solution for the nonlinear system of equations solved for the multiscale model, is considerably different from the final solution of the parameter values. This can lead to a failure of the minimization approach employed for the nonlinear system. Furthermore, this risk is enhanced when the hemodynamic computation is performed for pathologic cases, i.e. when the hemodynamic properties of the highest order model become more important compared to the properties of the 0D model. Secondly, the number of calibration iterations required to obtain the final solution for the parameter values increases. These repetitive computations increase the total execution time, an aspect which is a significant disadvantage when the calibration method is applied for patient specific computations in a clinical setting.

2.2. Proposed parameter estimation framework

We introduce a parameter estimation method which eliminates the drawbacks of the calibration method described in the previous section. An outline of the algorithm is illustrated in Fig. 1, which is composed of the steps described previously and two critical steps (displayed in bold: steps 6 and 7). One of the main advantages of the proposed algorithm is that it can be efficiently applied not only for healthy cases, but also for pathologic cases. The main idea is to efficiently account for the hemodynamic properties of the highest order model inside the multiscale model, when switching from the 0D model to the multiscale model. Particularly, we focus on two properties of the multiscale model: the compliance and the resistance.

At step 6, the compliance and resistances of the highest order model are estimated. These two quantities have not been taken into account when solving the nonlinear system of equations with the 0D model. Next, at step 7, the parameter values of the windkessel models are recomputed to account for the hemodynamic properties of the highest order model. Note that the values of the parameters of the nonlinear system are not modified at this stage and only the windkessel parameters are changed. The algorithms used for the estimation and compensation of the resistances and compliances are described in the next two subsections.

As a result of the two additional steps, the parameter estimation method adapts the overall properties of the multiscale models. For the multiscale computation, the windkessel parameters are the only quantities updated from one iteration to the next.

The parameter estimation methods do not always use the total resistances or the compliances as calibrated parameters. Nevertheless, regardless of the choice of parameters, the resistances and the compliances of the terminal windkessel models are always adapted when switching from the 0D model to the multiscale model. Additionally, if the resistances or the compliance of the multiscale model are adapted directly or indirectly, the parameters of the windkessel models are recomputed at the end of each iteration, based on the new parameter values determined through (9) and the estimated quantities of the highest order model. If the quantities are not adapted at all, then step 7 is applied only once (an aspect indicated by the dashed line in Fig. 1). The target objectives are: maximum pressure, $P_{\max}$, minimum pressure, $P_{\min}$, and flow rate split between outlets of the highest order model, Φ. The typical value of the residuals for pressure and flow-rate split objectives was set to 1 mmHg and 0.005 respectively.

2.3. Resistance estimation and compensation

To estimate the resistance of a healthy vascular segment for the highest order model, $(R_{HO})_i$, we assume a velocity profile:

$$(R_{HO})_i = \frac{2(\gamma+2)\mu}{\pi} \int_0^{L_i} \frac{1}{r_i^4(l)} dl \tag{10}$$

where γ is the power coefficient in the velocity profile $u = \bar{U}\frac{\gamma+2}{\gamma}[1-(\frac{r}{R})^{\gamma}]$, μ is the viscosity and r_i is the radius. For this work, we have chosen a parabolic profile ($\gamma = 2$) without any loss of generality. Alternatively a power law profile ($\gamma = 9$) or a Womersley profile [25] can be considered.

For a pathologic vascular segment (e.g. coarctation, stenosis) we use a comprehensive pressure-drop model to estimate the resistance of the pathological segment. This approach was validated against catheter-based ground-truth measurements in our previous work [23]. Since the time-varying flow rate through the descending aorta is not known apriori, the resistance of the CoA segment is computed from the average flow rate (which represents an objective of the parameter estimation method, i.e. it is known apriori):

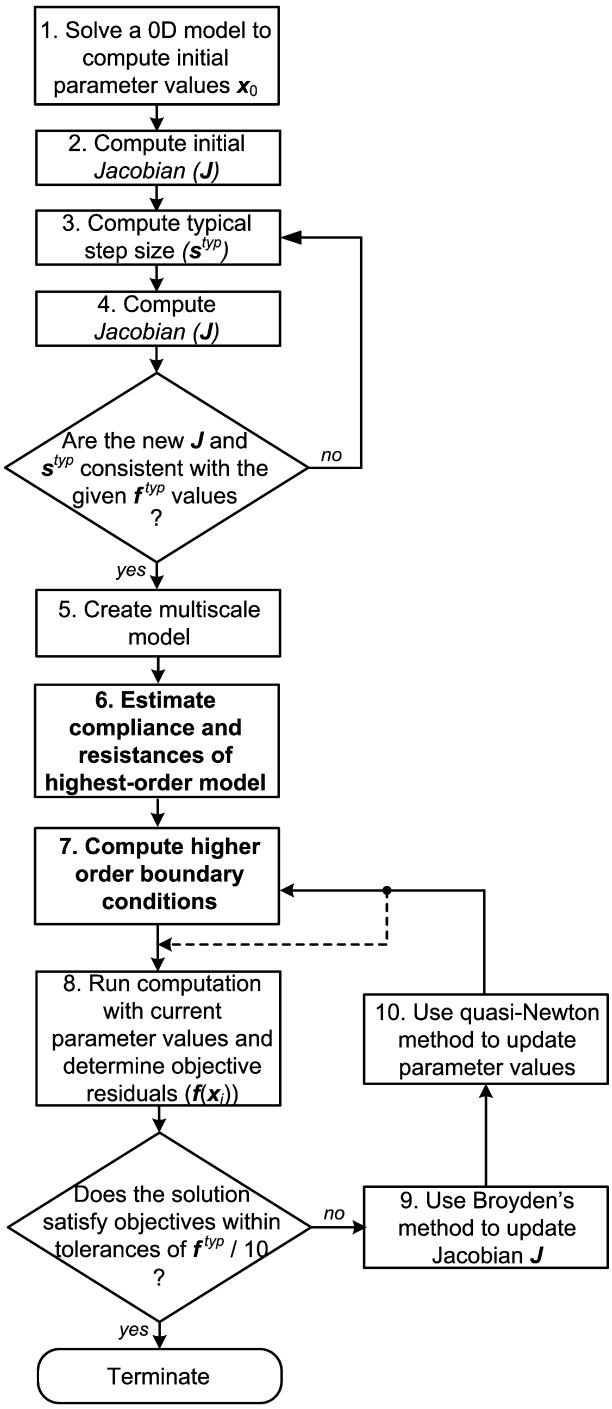

Fig. 1. The proposed parameter estimation method.

$$(R_{HO})_i = R_{CoA}(Q) = \Delta P(\bar{Q}_{DAo})/\bar{Q}_{DAo}, \tag{11}$$

where $\Delta P(\bullet)$ refers to the pressure drop model [23], and $\bar{Q}_{DAo}$ is the average flow rate through the descending aorta.

A similar approach can also be used if the multiscale model contains stenosed arteries. Depending on the region of interest, different pressure drop models have been proposed in the literature, e.g. coronary artery stenosis [26], femoral artery stenosis [27], renal artery stenosis [28]. For aneurysms, a different pressure drop model [29] can be applied to estimate the resistance.

Eqs. (10)–(11) are used at step 6 in Fig. 1 to determine the resistance of each branch of the multiscale model. Next, we introduce a recursive algorithm, employed at step 7, for adapting the total terminal resistances of the windkessel models, which is used during the switch from the 0D model to the multiscale model. Let n be the number of outlets in the geometric model, $(R_{t\text{-}0D})_j$ represents the total (sum of proximal and distal) resistance of the windkessel model used at each outlet ($j = 1..n$). The objective is to estimate the total resistances at each outlet of the geometric multiscale model $(R_{t\text{-}MS})_j$. Algorithm 1 illustrates the recursive function used for the resistance adaptation.

Algorithm 1. *adaptResistance* (totalRes, vesselNr)

$R_t \leftarrow$ totalRes
$i \leftarrow$ vesselNr
$(R_{t\text{-}MS})_i \leftarrow R_t - (R_{HO})_i$
if vessel i is a terminal vessel
    return
else

$$(R_{t\text{-}0D})_i \leftarrow 1 \Big/ \sum_k \frac{1}{(R_{t\text{-}0D})_k}, \quad k \rightarrow \text{terminal vessels downstream from vessel } i$$

    for each daughter vessel j of vessel i
        $\Phi_j \leftarrow (R_{t\text{-}0D})_i / (R_{t\text{-}0D})_j$
        $(R_{t\text{-}MS})_j \leftarrow (R_{t\text{-}MS})_i / \Phi_j$
        adaptResistance $((R_{t\text{-}MS})_j, j)$
    end (for)
end (if)
return

The function *adaptResistance* is called exactly once for the root segment of the arterial tree, which recursively computes all terminal resistances of the multiscale model. If the current segment is a terminal segment, the total terminal resistance is determined by subtracting the multiscale resistance of the current segment from the total resistance at the root of the vessel. If the current segment has daughter vessels, the goal is to distribute the new total resistance, $(R_{t\text{-}MS})_i$, to the outlets of segment i, in a manner that maintains the flow rate ratio in each daughter vessel. In the first step, the total resistance of the daughter vessels inside the 0D model is determined. Next, for each daughter vessel, using the ratio of total resistance of current vessel to terminal resistance of the current daughter vessel (Φ_j), the new terminal resistance of the current daughter vessel is determined ($(R_{t\text{-}MS})_j$). If the daughter vessel j is not a terminal vessel, $(R_{t\text{-}0D})_j$ is computed using the resistances of the downstream terminal vessels. Finally, function *adaptResistance* is called to further distribute the resistance of the current daughter vessel.

Eqs. (10)–(11) are used to estimate only once the resistance of each vascular segment. If the resistances are adapted directly or indirectly, Algorithm 1 is also applied, in a slightly modified version, at the end of each calibration iteration performed for the multiscale model (after computing the new parameter values through (9)). Hence, the total resistances of the 0D model used in Algorithm 1, $(R_{t\text{-}0D})_j$, are substituted by the total equivalent resistances of the multiscale model at each outlet of the highest order model, $(R_t)_j$, which is determined before applying the modified version of Algorithm 1. If the directly or indirectly adapted resistance refers to a single outlet, $(R_t)_j$ is set equal to this parameter value. Otherwise the parameter value is distributed to all outlets covered by the parameter. For the current study, we use a power law:

$$(R_t)_j = R_t \cdot \sum_k r_k^m / r_j^m, \tag{12}$$

where R_t refers to the adapted parameter, index k is used to iterate over all outlets covered by the adapted parameter and m is a power coefficient, whose physiological range of values is between two for large arteries [30] and three for small arteries [31].

2.4. Compliance estimation and compensation

To estimate the compliance of a vascular segment i of the highest order model in the multiscale model, $(C_{HO})_i$, we use the material properties of the arterial wall:

$$(C_{HO})_i = \int_0^{L_i} \frac{3\pi r_i^2(l)}{2} \cdot \frac{r_i(l)}{E_i \cdot h_i} dl, \tag{13}$$

where E_i is the Young's modulus and h_i is the wall thickness. Alternatively, also the method proposed by Ismail et al. [8] can be used. Most of the compliance in an arterial/venous tree resides in the large vessels, hence the compliance of the

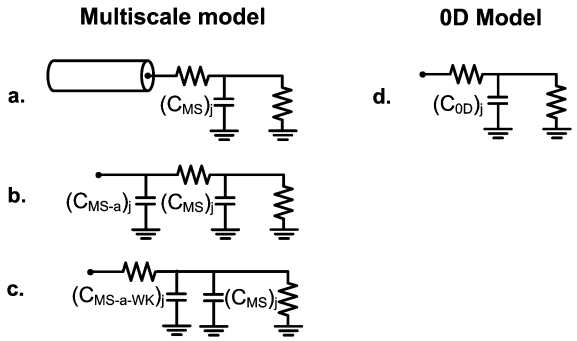

Fig. 2. (a) Classic representation of the multiscale model; (b) the compliance of the highest order model is lumped into a 0D compliance at outlet j placed before the windkessel model; (c) the compliance of the highest order model is ported inside the windkessel element; (d) classic representation of the windkessel model.

highest order model may become significant compared to the compliance of the windkessel elements, especially when using domains with large arteries. Next, the total compliance of the highest order model is determined $C_{HO} = \sum_i (C_{HO})_i$, which is then distributed to the outlets of the geometric model:

$$(C_{MS\text{-}a})_j = \left(C_{HO} \cdot r_j^2\right) \Big/ \sum_{j=1}^{n} r_j^2. \tag{14}$$

where $(C_{MS\text{-}a})_j$ represents the assumed additional compliance introduced at each outlet of the highest order model inside the multiscale model. The goal is to determine the compliance of the windkessel models, $(C_{MS})_j$, so as to obtain for the multiscale model the same total compliance as the one used for the 0D model, $(C_{0D})_j$. Fig. 2 introduces different representations for the compliance of the multiscale model, alongside the 0D model.

Fig. 2(a) displays the classic representation of the multiscale model, composed of the highest order model and the terminal windkessel element. In Fig. 2(b), the compliance of the highest order model is lumped into a 0D compliance at outlet j, $(C_{MS\text{-}a})_j$, placed before the windkessel model. To determine the compliances of the windkessel elements of the multiscale model, $(C_{MS})_j$, $(C_{MS\text{-}a})_j$ is ported inside the windkessel model, as displayed in Fig. 2(c). For the models in Fig. 2(c) and Fig. 2(d) to be equivalent, the following relationship must hold:

$$(C_{MS})_j = (C_{0D})_j - (C_{MS\text{-}a\text{-}WK})_j. \tag{15}$$

Hence, to determine $(C_{MS})_j$, $(C_{MS\text{-}a\text{-}WK})_j$ must be computed. $(C_{MS\text{-}a\text{-}WK})_j$ represents the assumed additional compliance introduced by the multiscale model at outlet j and ported inside the three-element windkessel model. Three different approaches were tested for computing $(C_{MS\text{-}a\text{-}WK})_j$.

Approach 1 – Direct compliance compensation. The influence of the proximal resistance of the windkessel model is neglected:

$$(C_{MS\text{-}a\text{-}WK})_j = (C_{MS\text{-}a})_j. \tag{16}$$

Approach 2 – Analytical compliance compensation. Approach 1 does not take into account the fact that the proximal resistance of the windkessel element diminishes the influence of the compliance. Thus, following a method proposed previously [32]:

$$(C_{MS\text{-}a\text{-}WK})_j = (C_{MS\text{-}a})_j / \left(1 - (R_{p\text{-}MS})_j / (R_{t\text{-}MS})_j\right), \tag{17}$$

where $(R_{p\text{-}MS})_j$ is the proximal resistance of the windkessel model at outlet j of the highest order model.

Approach 3 – Numerical compliance compensation. Thirdly, we propose a numerical approach based on the pulse pressure method (PPM) [33], which is described in Algorithm 2. PPM has been introduced to estimate the compliance downstream of a location in an arterial tree, at which the time-varying flow rate values and the average and pulse pressure are known. In the following we use a modified PPM, based on a three-element windkessel model (PPM-WK3) which replaces the two-element windkessel model in the original PPM.

Algorithm 2. *PPM-based compliance compensation*

for each terminal vessel j

Run computation with two element WK model $((Q_{0D}(t))_j, (R_{t\text{-}MS})_j, (C_{MS\text{-}a})_j) \rightarrow (PP_{\text{ref}})_j$

Initialize PPM-WK3 $\rightarrow (Q_{0D}(t))_j$, $(R_{p\text{-}MS})_j$, $(R_{d\text{-}MS})_j$, $(C_{MS\text{-}a})_j$, $(PP_{\text{ref}})_j$

Run PPM-WK3 $\rightarrow (C_{MS\text{-}a\text{-}PPM})_j$

$(C_{MS\text{-}a\text{-}WK})_j \leftarrow (C_{MS\text{-}a\text{-}PPM})_j$

end (for)

First, a two-element windkessel model is used to determine a reference pulse pressure, $(PP_{\text{ref}})_j$, using the flow rate profile obtained at outlet j of the highest order model during the last computation performed with the 0D model, $(Q_{0D}(t))_j$, the total resistance at outlet j after resistance compensation, $(R_{t\text{-}MS})_j$, and the assumed additional compliance introduced at outlet j, $(C_{MS\text{-}a})_j$. Next, PPM-WK3 is initialized and run, and as a result the compliance value, to be subtracted in Eq. (15) from the compliance used inside the 0D model, is determined.

Approaches 1–3 are used to estimate only once the assumed additional compliance introduced by the multiscale model at each outlet j of the highest order model. If the compliance of the multiscale model is adapted directly or indirectly, the compliance values of the windkessel elements are recomputed at each calibration iteration performed for the multiscale model. In this case, considering C the total compliance of the multiscale model, this value is first distributed to the outlets of the highest order model, using a relationship similar to (14):

$$(C_{MS\text{-}t})_j = \left(C \cdot r_j^2\right) \Big/ \sum_{j=1}^{n} r_j^2, \tag{18}$$

where $(C_{MS\text{-}t})_j$ represents the total equivalent compliance of the multiscale model at each outlet of the highest order model.

For the recomputation of the windkessel compliance, a relationship similar to (15) is employed:

$$(C_{MS})_j = (C_{MS\text{-}t})_j - (C_{MS\text{-}a\text{-}WK})_j. \tag{19}$$

Compliance compensation is always performed after resistance compensation.

3. Results

To evaluate the performance of the proposed parameter estimation method, next we present results for patient-specific and multiple idealized anatomical models representing distinct arterial segments, and for a full body arterial model. The first case is a patient-specific aortic coarctation model extracted from MRI images. The parameter estimation method ensures that the computational setup is personalized, and, consequently, computed pressure and flow values are in close agreement with the clinical measurements. The second case is a full body arterial model, whereas the parameter estimation method ensures that the computed systolic and diastolic pressure values, and the average flow rate distribution to each outlet of the highest order model match the reference values. The remaining cases are based on idealized arterial geometries [7], to analyze the role of different cost-functions and constraints.

Results are reported for four different parameter estimation methods: the calibration method for windkessel parameters (WKC) [7], the parameter estimation method with resistance compensation and Direct Compliance compensation (DC), the parameter estimation method with resistance compensation and Analytical Compliance compensation (AC), and the parameter estimation method with resistance compensation and Numerical Compliance compensation (NC).

Blood is modeled as an incompressible Newtonian fluid with a density of 1.050 g/cm^3 and a dynamic viscosity of 0.040 dynes/(cm^2 s). The grid size is 0.05 cm, while the time-step (limited by the CFL-condition) is set equal to 2.5e−5s.

3.1. Patient-specific flow computation for aortic coarctation

Several CFD-based methods for non-invasive assessment of trans-stenotic pressure gradient have been proposed recently [23,34–36]. For an accurate patient-specific estimation, the CFD-based solution should be in close agreement with the measured pressure and flow-data, a task that requires automatic calibration of the boundary conditions.

The patient-specific anatomical model [37] is composed of the ascending aorta, three supra-aortic branches, aortic arch, coarctation, and the descending aorta (Fig. 3(a)). Fig. 3(b) displays the multiscale model corresponding to the CoA patient-specific geometry. A measured flow rate profile is provided at the inlet, while time-averaged flow-splits are provided for each of the outlets of the geometric model. The objective is to compute the pressure drop across the coarctation, under the constraint that the CFD-based solutions should i) maintain the same flow-split at each outlet as with the measured data, and ii) replicate the measured systolic and diastolic pressure in the aorta. Fig. 3(c) displays the corresponding 0D model.

To build the discretized geometric mesh required for the blood flow computation, we first used the vascular modeling toolkit (vmtk [38]) to extract the centerline and the cross-sectional areas along the centerline of each arterial segment. Next we used an approach similar to previously introduced ones [39], wherein for each vessel of the arterial model, we used several distinct 1D segments with spatially varying cross-sectional area values in order to obtain a geometry close to the 3D geometry acquired through MRI.

Given the high compliance of the ascending aortic wall, this example underlines the advantages of a compliance compensation. At the same time, it also demonstrates the advantages of the resistance compensation for high resistance segments, such as the coarctation.

The parameters to be estimated are the total resistances of the three supra-aortic vessels and of the descending aorta, and the total compliance. The following system of nonlinear equations is numerically solved to obtain the optimum value of each parameter:

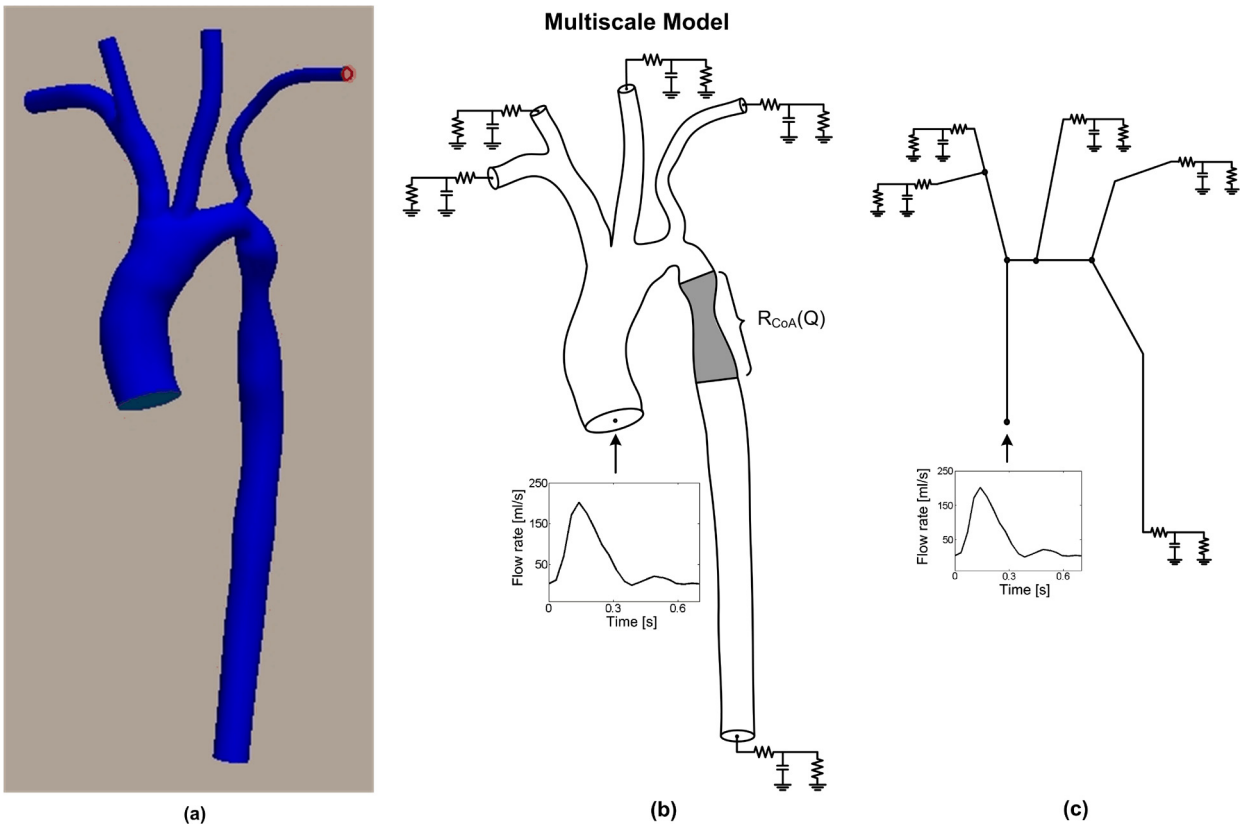

Fig. 3. (a) Proximal aorta geometry with coarctation, (b) Multiscale model used for determining the windkessel parameter values of the patient-specific model, (c) 0D model used during the first steps of the model personalization algorithm for finding an initial solution of the parameter values.

$$\boldsymbol{f}\begin{pmatrix} R_{t\text{-}BC} \\ R_{t\text{-}LCC} \\ R_{t\text{-}LS} \\ R_{t\text{-}DAo} \\ C \end{pmatrix} = \begin{Bmatrix} (P_{\max})_{comp} - (P_{\max})_{ref} \\ (P_{\min})_{comp}(P_{\min})_{ref} \\ (\Phi_{BC})_{comp} - (\Phi_{BC})_{ref} \\ (\Phi_{LCC})_{comp} - (\Phi_{LCC})_{ref} \\ (\Phi_{DAo})_{comp} - (\Phi_{DAo})_{ref} \end{Bmatrix} = \begin{Bmatrix} 0 \\ 0 \\ 0 \\ 0 \\ 0 \end{Bmatrix}, \tag{20}$$

where $P_{\max}$ is the maximum (systolic) pressure, $P_{\min}$ is the minimum (diastolic) pressure, $(\Phi)_{\bullet}$ represents a flow rate split, while $(\bullet)_{comp}$ refers to a value computed using the 0D/Multiscale model, and $(\bullet)_{ref}$ refers to the reference value. Index *BC* refers to the brachiocephalic artery, *LCC* to the left common carotid artery and *DAo* to the descending aorta. The reference systolic and diastolic pressures (115 mmHg and 65 mmHg respectively), and the reference flow-rate splits are taken from literature data [37]. Only three of the four flow rate splits are used as objectives in (20) since the fourth one is obtained as difference. The characteristics of the pressure waveform are determined at the outlet of the left subclavian artery [36].

One of the estimated total resistances corresponds to several outlets ($R_{t\text{-}BC}$ represents the equivalent total resistance of the right subclavian artery and the right common carotid artery). Hence, before applying Algorithm 1, at the end of the calibration iterations performed for the multiscale model, the total equivalent resistance of the multiscale model at each of the two outlets of the brachiocephalic artery is determined using (12), with a power coefficient equal to two. The proximal resistance of each windkessel model is set equal to the characteristic resistance and was maintained constant throughout the parameter estimation method.

Since total resistance is adapted directly, Algorithm 1 is applied both when switching from the 0D model to the multi-scale model, and during each additional calibration iteration performed for the multiscale model. Since compliance is also adapted directly, (14) and (15) are used for the initial compliance compensation, and (18) and (19) are applied at each further calibration iteration.

The objective and parameter values obtained with the four different parameter estimation methods are displayed in Fig. 4. Whereas three iterations are required with the WKC method, two iterations are required with the DC and AC methods, and only one iteration is required with the NC method.

With any of the proposed parameter estimation methods, the objective and parameter values are significantly closer to their reference/final values. When the WKC method is used, the pulse pressure at iteration 0 is significantly smaller than the reference pulse pressure, caused by the additional compliance of the highest order model (especially the initial diastolic pressure is considerably closer to the final value). This aspect is also reflected by the fact that the compliance value at

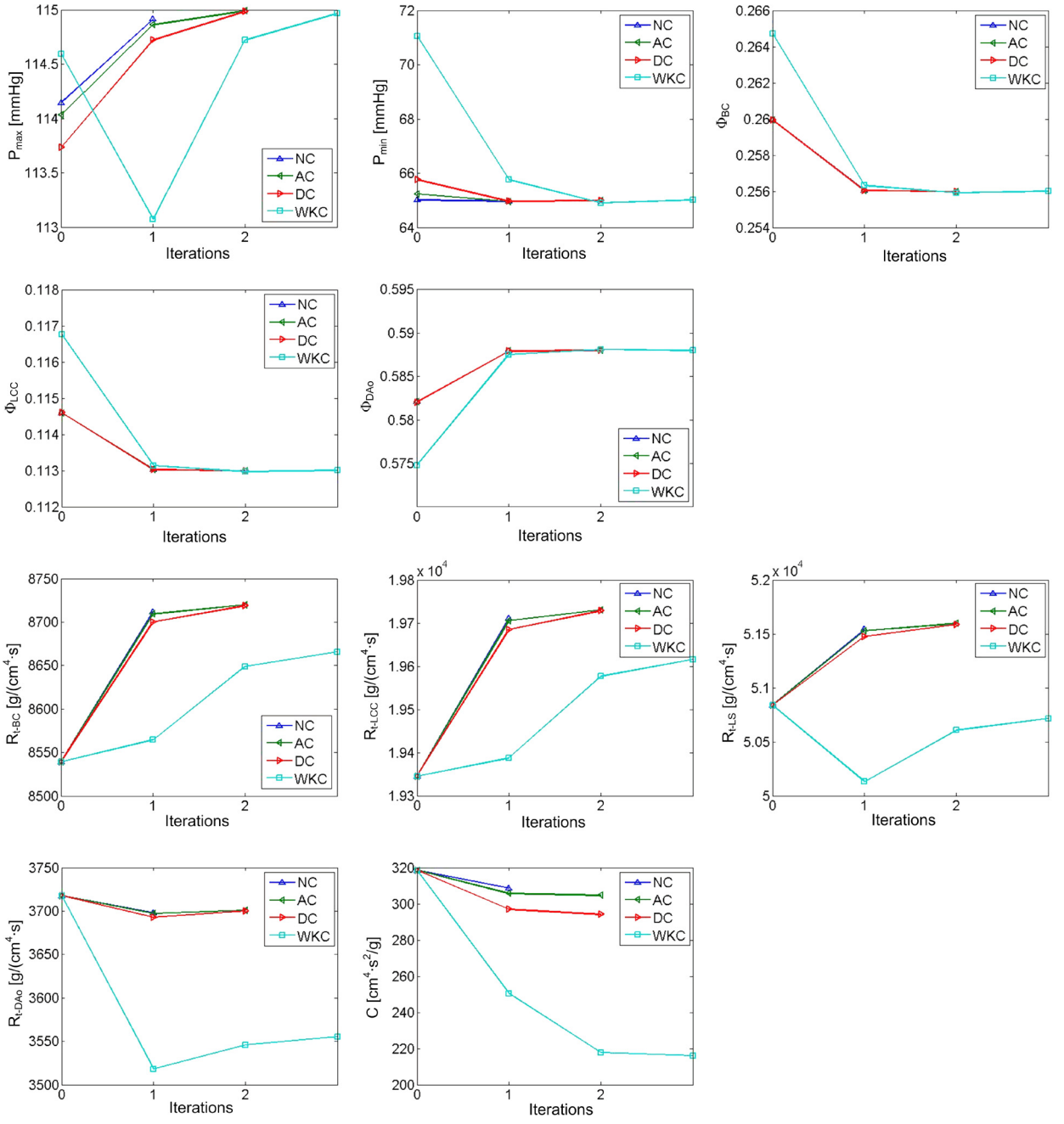

Fig. 4. Parameter estimation progression for the proximal aorta model. The total resistance of each of the three supra-aortic branches, the total resistance of the descending aorta windkessel model and the sum of all compliances were the adapted parameters. The desired mean fractions of flow through supra-aortic branches and through the descending aorta were used as objectives, besides systolic and diastolic pressure.

iteration 0 is significantly closer to its final value for the proposed methods. Furthermore all initial computed flow rate split values are closer to their final values. This is mainly caused by the significantly improved initial estimate of the total resistance on the descending aorta $R_{t\text{-}DAo}$.

As opposed to the objectives, where the final values are identical for all four parameter estimation methods, the final parameter values are different for the two methods. This is caused by the fact that the herein introduced methods adapt the overall properties of the multiscale model, whereas the WKC method adapts directly the parameters of the three-element windkessel models. Hence, although the parameter values of the two methods at iteration 0 are identical, the values of the windkessel parameters are in fact different. The initial estimate of $R_{t\text{-}DAo}$ for the proposed parameter estimation methods is superior since (11) is employed for computing the resistance of the CoA segment.

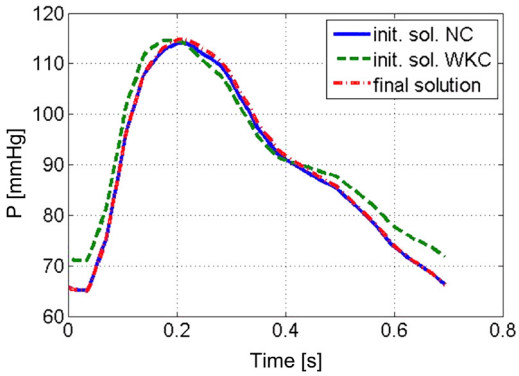

Fig. 5. Comparison of the pressure profiles at the outlet of the left subclavian artery of the proximal aorta model, corresponding to the initial solution of the NC method, the initial solution of the WKC method and the final solution.

Table 1
Comparison of reference and computed flow rate split values.

Artery	Reference flow split [%]	Computed flow split (NC) [%]
Brachiocephalic artery	25.6	25.6044
Left common carotid artery	11.3	11.3022
Left subclavian artery	4.26	4.3009
Descending aorta	58.8	58.7925

Table 2
Final values of the adapted parameters for four different parameter estimation methods applied for the nonlinear system in (20).

Parameter estimation method	$(R_{t-BC})_{\text{final}}$ [g/(cm^4 s)]	$(R_{t-LCC})_{\text{final}}$ [g/(cm^4 s)]	$(R_{t-LS})_{\text{final}}$ [g/(cm^4 s)]	$(R_{t-DAo})_{\text{final}}$ [g/(cm^4 s)]	$(C)_{\text{final}}$ [10^{-6} cm^4 s^2/g]
NC	8711.3	19 710.6	51 541.6	3698.0	308.71
AC	8720.0	19 730.8	51 595.4	3700.7	304.63
DC	8718.8	19 728.2	51 587.6	3700.0	294.18
WKC	8665.7	19 615.9	50 715.9	3555.4	216.14

Table 3
Compensated CoA resistance and compliance values for four different parameter estimation methods applied for the nonlinear system in (20) (RS – right subclavian artery, RCC – right common carotid artery, LCC – left common carotid artery, LS – left subclavian artery).

Parameter estimation method	R_{CoA} [g/(cm^4 s)]	$C_{MS-a-WK}$ [10^{-6} cm^4 s^2/g]				
		RS	RCC	LCC	LS	DAo
NC	125.17	18.15	9.679	13.23	5.830	45.68
AC	125.17	17.45	0.245	12.77	5.442	44.37
DC	125.17	15.44	8.097	11.48	4.700	38.85
WKC	0.0	0.0	0.0	0.0	0.0	0.0

Fig. 5 displays a comparison of the pressure profiles at the outlet of the left subclavian artery, corresponding to the initial solution of the WKC method, the initial solution of the NC method and the final solution (identical for both parameter estimation methods). The initial solution refers to the results obtained at iteration zero with the multiscale model. The initial solution provided by the NC method is clearly superior to the initial solution provided by the WKC method and almost identical to the final solution.

Table 1 compares the reference and the computed flow rate split values (obtained with the NC method): the values match almost perfectly. Table 2 and Table 3 display for each parameter estimation method the final values of the adapted parameters and the compensated multiscale compliance and CoA resistance values respectively. The compensated compliance is highest for the NC method. Importantly, the sum of the five compensated compliance values reflects the difference between the final total compliance values obtained with the proposed parameter estimation methods and with the WKC method. Furthermore, the compensated CoA resistance (R_{CoA}) roughly reflects the difference between the final total resistance value on the descending aorta (R_{t-DAo}) obtained with the proposed methods and with the WKC method.

The computed average pressure drop across the coarctation is 4.12 mmHg, while the peak pressure difference is of 16.88 mmHg, both in the range of the values reported for the challenge [36].

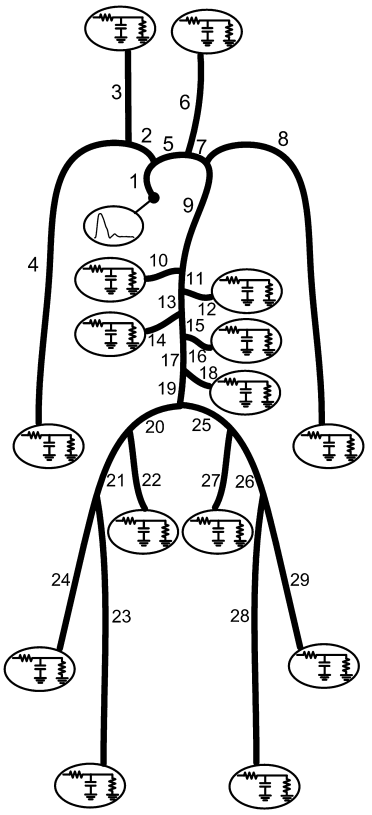

Fig. 6. The full body arterial model composed of 29 arteries [15]. A time-varying flow rate profile is prescribed at the inlet, while the microcirculation downstream from each outlet is lumped into three-element windkessel models.

3.2. Full body arterial flow computation

One-dimensional blood flow models have been shown to be able to accurately predict pressure and flow rate waveforms in full body arterial flow computations. The full body arterial model used herein is composed of 29 arteries (Fig. 6) [15]. The objectives of the parameter estimation procedure were the maximum pressure (128 mmHg), the minimum pressure (70 mmHg) – both determined in the left subclavian artery, and the flow rate split values at the 15 outlets of the geometric model (the reference values were taken from [15]). Only fourteen of the fifteen flow rate splits are used as objectives since the fifteenth one is obtained as difference.

The parameters to be estimated are the total resistance at each outlet and the ratio of proximal to total resistance (the same ratio is used at each outlet). The following system of nonlinear equations is numerically solved to obtain the optimum value of each parameter:

$$\boldsymbol{f}\begin{pmatrix} R_{t3} \\ R_{t4} \\ \cdots \\ R_{t28} \\ R_{t29} \\ \rho \end{pmatrix} = \begin{Bmatrix} (P_{\max})_{comp} - (P_{\max})_{ref} \\ (P_{\min})_{comp} - (P_{\min})_{ref} \\ (\Phi_3)_{comp} - (\Phi_3)_{ref} \\ (\Phi_4)_{comp} - (\Phi_4)_{ref} \\ \cdots \\ (\Phi_{28})_{comp} - (\Phi_{28})_{ref} \end{Bmatrix} = \begin{Bmatrix} 0 \\ 0 \\ 0 \\ 0 \\ 0 \\ 0 \end{Bmatrix}, \tag{21}$$

where $P_{\max}$ is the maximum (systolic) pressure, $P_{\min}$ is the minimum (diastolic) pressure, $(\Phi)_\bullet$ represents a flow rate split. Indices 3 to 29 refer to the outlets in the geometric model. $(P_{\max})_{comp}$ and $(P_{\min})_{comp}$ were determined in the middle of segment 8.

Since total resistance is adapted directly, Algorithm 1 is applied both when switching from the 0D model to the multiscale model, and during each additional calibration iteration performed for the multiscale model. The compliance is not adapted, neither directly or indirectly. Hence, compliance compensation is performed only once, through (14) and (15).

The first three objective and parameter values obtained with the four different parameter estimation methods are displayed in Fig. 7. Whereas four iterations are required with the WKC method, only three iterations are required with the NC, AC and DC methods.

With any of the proposed methods the objective and the parameter values are significantly closer to their reference/final values. When the WKC method is used, the pulse pressure at iteration 0 is significantly smaller than the reference pulse

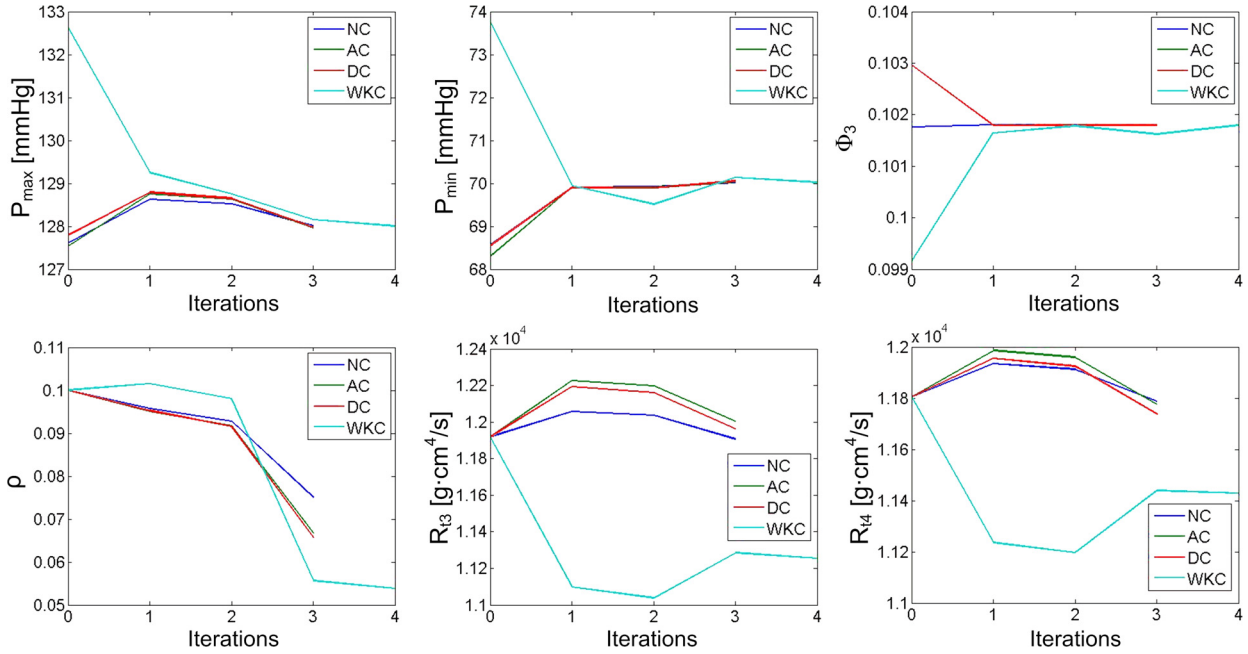

Fig. 7. Parameter estimation progression for the full body arterial model. The total resistance at each outlet of the geometric model and the proximal resistance fraction were the adapted parameters. Systolic pressure, diastolic pressure and the desired mean fractions of flow through each outlet were used as objectives.

Table 4
Compensated multiscale compliance values at each outlet of the geometric model and final proximal resistance fraction values for four different parameter estimation methods, WKC, DC, AC and NC, applied for the nonlinear system in (21).

Quantity	Branch	NC	AC	DC	WKC
$C_{MS\text{-}a\text{-}WK}$ [10^{-6} cm^4 s^2/g]	3	31.436	24.951	22.257	0.0
	4	26.136	20.944	18.758	0.0
	6	26.141	20.956	18.758	0.0
	8	31.391	24.956	22.257	0.0
	10	33.255	25.981	23.366	0.0
	12	35.748	28.110	25.272	0.0
	14	23.500	18.336	16.487	0.0
	16	23.500	18.337	16.487	0.0
	18	12.038	9.364	8.412	0.0
	22	13.340	10.667	9.571	0.0
	23	14.292	10.678	9.571	0.0
	24	48.246	32.444	29.076	0.0
	27	13.448	10.663	9.571	0.0
	28	14.830	10.673	9.571	0.0
	29	53.124	32.427	29.076	0.0
$(\rho)_{\text{final}}$	–	0.06669	0.06569	0.075111	0.053852

pressure, caused by the additional compliance of the highest order model. The initial computed flow rate split values are closer to their final values, an aspect which is determined by the resistance estimation and compensation.

Table 4 displays for the parameter estimation methods the compensated multiscale compliance at each outlet of the geometric model and the final values of the proximal resistance fraction. At each outlet the compensated compliance is highest for the NC method and the final value of the proximal resistance fraction is closer to the initial value (0.1) for the proposed methods, compared to the WKC method.

3.3. Idealized artery models

To analyze the role of different cost-functions and constraints, and characterize the performance of the proposed model personalization algorithms, next we present brief results on four idealized arterial geometries. For the first three calibration processes, different parameters of an idealized common carotid artery model were adapted to achieve desired maximum and minimum pressure values (Fig. 8(a)), set to 120 mmHg and 80 mmHg respectively. The fourth calibration process focuses on an idealized iliac arterial bifurcation and adds a third objective in terms of the average flow rate split between the

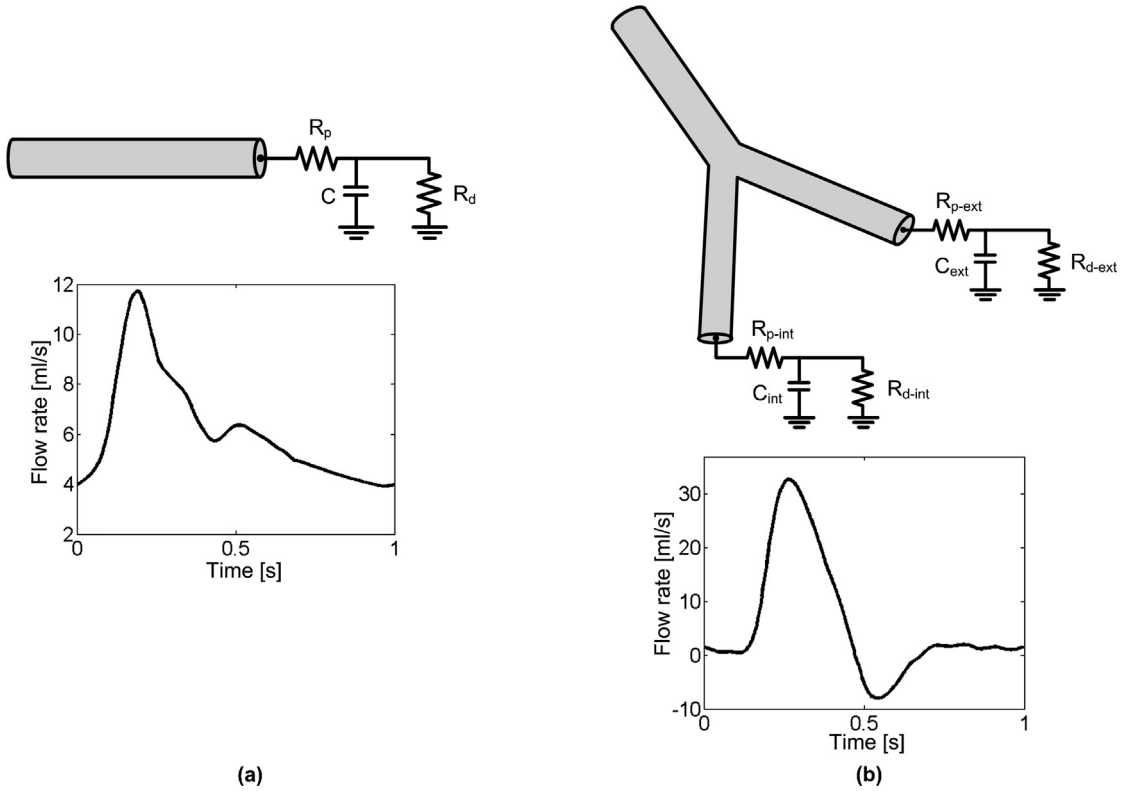

Fig. 8. (a) Idealized common carotid artery model and corresponding inlet flow rate profile; (b) Idealized iliac bifurcation model and corresponding inlet flow rate profile.

two daughter vessels (Fig. 8(b)). The characteristics of the pressure waveform are determined at the inlet of the multiscale model, and a Young's modulus of $5 \cdot 10^6$ g/(cm s^2) and a vessel wall thickness of 0.1 cm were used.

The system of nonlinear equations for the common carotid artery model is formulated as follows for the three different calibration configurations:

$$\boldsymbol{f}\begin{pmatrix} R_t \\ C/\rho/\tau \end{pmatrix} = \begin{Bmatrix} (P_{\max})_{comp} - (P_{\max})_{ref} \\ (P_{\min})_{comp} - (P_{\min})_{ref} \end{Bmatrix} = \begin{Bmatrix} 0 \\ 0 \end{Bmatrix}, \tag{22}$$

whereas the total resistance and the compliance, the proximal resistance fraction or the time constant of the windkessel model are used as adapted parameters. When the compliance is adapted directly (the proximal resistance fraction is fixed), (15) and (16) are used for the initial compliance compensation, and (19) and (20) are applied at each further calibration iteration. When the proximal resistance fraction is used as calibration parameter, the compliance is not adapted, neither directly or indirectly. Hence, compliance compensation is performed only once, through (14) and (15). Finally when the time constant is calibrated, since the time constant is given by the compliance and the distal resistance, compliance is adapted indirectly.

With any of the proposed methods, the objective and parameter values are significantly closer to their reference/final values (Fig. 9 displays the objective and parameter values for the first configuration). Table 5 displays for each configuration and parameter estimation method the final values of the adapted parameters and the compensated multiscale compliance and resistance values respectively. Only one iteration is required with the DC, AC and NC methods whereas two or three iterations are required for the WKC method.

For the first calibration configuration, the compensated multiscale compliance is highest for the NC method, and, overall, the compensated multiscale compliances reflect the difference between the final total compliance values obtained with the proposed methods and with the WKC method.

For the second calibration configuration, the additional compliance introduced by the highest order model leads to significant changes for the proximal resistance ratio, which is increased substantially by the WKC method. Note that a higher proximal resistance ratio leads to a smaller effective compliance for the windkessel model. Hence, the WKC method compensates for the additional compliance by increasing the proximal resistance ratio.

For the third calibration configuration, the additional compliance introduced by the highest order model leads to significant changes for the time constant, which is decreased substantially for the WKC method. This aspect can be explained as follows: the time constant is directly proportional to the compliance, and, since the distal resistance of the windkessel

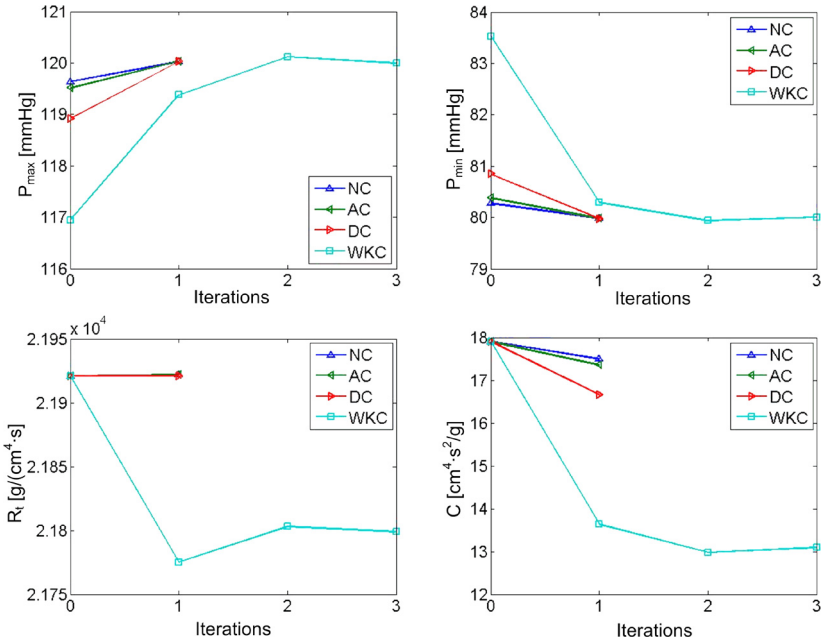

Fig. 9. Parameter estimation progression for the common carotid artery model with a chosen proximal resistance fraction. The total resistance and the compliance of the windkessel model were the adapted parameters. Reference systolic and diastolic pressures were the objectives. Results are compared for four different parameter estimation methods: WKC, DC, AC and NC.

Table 5
Final values of the calibrated parameters and of the compensated quantities for four different parameter estimation methods, WKC, DC, AC and NC, applied for the nonlinear system in (22) representing three different configurations of the common carotid artery.

Calibration parameters	Parameter estimation method	$(R_t)_{\text{final}}$ [g/(cm^4 s)]	$(C)_{\text{final}}$ [10^{-6} cm^4 s^2/g]	$(\rho)_{\text{final}}$	$(\tau)_{\text{final}}$ [s]	R_{HO} [g/(cm^4 s)]	$C_{MS\text{-}a\text{-}WK}$ [10^{-6} cm^4 s^2/g]	Iterations
R_t and C	NC	21 921	17.494	0.1600	0.32213	122.27	4.430	1
	AC	21 921	17.353	0.1600	0.31953	122.27	4.293	1
	DC	21 921	16.666	0.1600	0.30688	122.27	3.606	1
	WKC	21 799	13.091	0.1600	0.23971	0.0	0.0	3
R_t and ρ	NC	21 913	15.000	0.0764	0.30358	122.27	3.856	1
	AC	21 913	15.000	0.0771	0.30335	122.27	3.841	1
	DC	21 915	15.000	0.0878	0.29986	122.27	3.606	1
	WKC	21 802	15.000	0.2158	0.25646	0.0	0.0	2
R_t and τ	NC	21 922	17.563	0.1600	0.32342	122.27	4.463	1
	AC	21 923	17.412	0.1600	0.32065	122.27	4.316	1
	DC	21 922	16.706	0.1600	0.30763	122.27	3.606	1
	WKC	21 799	13.151	0.1600	0.24081	0.0	0.0	3

model is given by the constant proximal resistance ratio and by the total resistance, a smaller time constant is equivalent to a smaller compliance. Hence, the WKC method compensates for the additional compliance by decreasing the time constant.

For the iliac bifurcation, the system of nonlinear equations was formulated as follows:

$$\boldsymbol{f}\begin{pmatrix} R_{t\text{-}ext} \\ R_{t\text{-}int} \\ \rho \end{pmatrix} = \begin{Bmatrix} (P_{\max})_{comp} - (P_{\max})_{ref} \\ (P_{\min})_{comp} - (P_{\min})_{ref} \\ (\Phi)_{comp} - (\Phi)_{ref} \end{Bmatrix} = \begin{Bmatrix} 0 \\ 0 \\ 0 \end{Bmatrix}. \tag{23}$$

The reference flow rate split value was determined based on the square law of the radiuses [30] for large arteries: $(\Phi)_{ref} = Q_{ext}/(Q_{ext} + Q_{int}) = 0.719$. The compliances at the two outlets of the highest order model are chosen and are not adapted, neither directly or indirectly.

Whereas two iterations were required with the WKC method, only one iteration was required with the DC, AC and NC methods. The final value of parameter ρ is higher for the WKC method (Table 6).

Table 6
Final values of the adapted parameters and of the compensated compliance for four different parameter estimation methods applied for the nonlinear system in (23).

Parameter estimation method	$(R_{t-ext})_{\text{final}}$ [g/(cm^4 s)]	$(R_{t-int})_{\text{final}}$ [g/(cm^4 s)]	$(\rho)_{\text{final}}$	$C_{MS-a-WK}$ [10^{-6} cm^4 s^2/g]		Iterations
				Ext. Iliac	Int. Iliac	
NC	30 625	78 360	0.050129	3.376	1.319	1
AC	30 625	78 360	0.050133	3.371	1.316	1
DC	30 621	78 349	0.050239	3.222	1.258	1
WKC	30 450	77 736	0.052197	0.0	0.0	2

4. Discussion

The results presented in the previous section demonstrate the advantages of the model personalization algorithm, which leads to superior calibration results for the patient-specific CoA geometry, the full body arterial model and the idealized arterial models. The initial solutions with the multiscale models are improved for all six configurations and the number of calibration iterations is reduced by a factor of up to 3. The DC and AC methods are easier to implement and computationally faster due to their analytical nature. Given the high computational cost associated with multiscale models, the additional execution time for the NC method, compared to the DC and AC methods, is negligible. Since the NC method has the best performance, we consider this variant of the proposed parameter estimation method to be the most efficient. Note that the configurations of the 0D model and the multiscale model are not affected by the additional steps in the proposed parameter estimation method, and the framework developed for the WKC method can be completely reused.

The geometrical multiscale framework for the aortic model is useful for modeling multiple pathologies. Recently, we validated (with in-vivo measurements) a reduced-order multiscale model for the non-invasive assessment of aortic coarctation [23]. A fully automated parameter estimation method was proposed for personalizing the hemodynamic computations. The goals of this estimation method were to match the patient-specific average aortic pressure, the flow distribution between supra-aortic arteries and the descending aorta, and to determine the aortic wall properties. Excellent validation results were obtained for the non-invasive computation of the trans-coarctation peak-to-peak pressure-gradient.

The configuration used in the previous section for the CoA geometry provides the possibility to enhance the personalization of the hemodynamic computations by matching not necessarily the mean arterial pressure, computed from the systolic and diastolic pressure, but directly the two cuff-based pressures. Matching the flow rate split for the descending aorta is crucial since the trans-coarctation pressure-drop is highly dependent on the flow rate through the descending aorta. Previously only the average flow rate was considered, but, using an automated parameter estimation method, the maximum and/or minimum flow rate can also be constrained.

The proposed parameter estimation method provides significant advantages when the multiscale model is an FSI model (when rigid wall models are used, only the resistance compensation is required). For the non-invasive assessment of aortic coarctation FSI modeling is required: since the trans-coarctation pressure gradient is computed as a peak-to-peak pressure difference between the ascending aorta and the descending aorta, the pressure drop is not mainly determined by the maximum flow rate and the geometry, but by the complex interaction between these two aspects, the phase lag introduced by the compliance, the wave propagation speed, and the backward traveling pressure and flow rate waves. Furthermore, the wall properties can also be used as adapted parameters in order to match a specific feature of the wave propagation aspects.

The configuration used in the previous section for the full body arterial model indicates that minimization based methods perform well even when the number of calibrated parameters is relatively high (16 parameters are used in (21)). The parameters used in (21) represent directly adapted parameters. In fact, all resistances of the windkessel models are calibrated, not independently, but indirectly through the total resistance values and the proximal resistance fraction. Moreover, by calibrating the proximal resistance fraction, the impact of the compliances of the windkessel models is also changed. Hence although only 16 parameters are calibrated directly, in fact the impact of all 45 windkessel parameters is adapted by applying the parameter estimation methods. To be able to calibrate more parameters directly, a higher number of patient-specific measurements is required.

Parameter estimation methods for model personalization are not only useful for performing patient-specific computations using measured data, but also to perform computations for other conditions, like exercise, drug-induced hyperemia, or post surgical intervention. Patient-specific computations for CoA patients corresponding to the exercise state were reported previously [35], where time-varying and average trans-coarctation pressure gradient, wall shear stress and oscillatory shear index parameters were analyzed. Parameter estimation methods provide the possibility to enhance the value of such (predictive) computations by imposing different changes for the reference values, compared to the rest state. For example, different elevations of mean or systolic aortic pressure, or of flow rate through the descending aorta could be imposed. Such an approach would eliminate the risks and the costs involved in measuring these quantities in-vivo. Regarding treatment planning evaluation, parameter estimation methods are useful for imposing a certain post-interventional state for the hemodynamic computation, which then enables an accurate assessment of the treatment options.

Our study has a series of limitations. The parameter estimation method has only been tested with a reduced-order multiscale model and not with a full-order multiscale model. The procedures proposed for the estimation and compensation of

the resistances and compliances though can also be applied for the calibration procedures performed with full-order multiscale models. The velocity profile of the reduced-order model was known apriori, leading thus to good estimations of the resistance through (10). With a full-order model, the velocity profiles are not known apriori and, for unsteady simulations, the resistances should be estimated using a Womersley profile. On the other hand though, we have seen that from the two hemodynamic properties considered, the compensation of the compliance is more important than the compensation of the resistance for improving the calibration results (unless a pathologic vessel is encountered, case in which a different approach is used for estimating the resistance). Furthermore, the inertance, a third important hemodynamic property, alongside resistance and compliance, has not been considered when switching from the 0D model to the multiscale model. The inertance effects are particularly important in the large arteries and the compensation of this property could lead to better initial solutions with the multiscale model.

5. Conclusions

In this paper, we have introduced a fully automated parameter estimation method for personalizing geometrical multiscale blood flow computations in healthy and pathologic arterial geometries.

Three different variants of the proposed parameter estimation method were evaluated on a patient-specific aorta model with coarctation, a full body arterial model and four idealized arterial geometries. The best performing method was the parameter estimation method with resistance compensation and numerical compliance compensation, which is based on a modified pulse pressure method for the estimation of the compliances of the highest order model. The number of calibration iterations with the geometrical multiscale model was reduced for all six configurations considered herein.

Acknowledgements

This work is partially supported by the program Partnerships in Priority Domains (PN II), financed by ANCS, CNDI-UEFISCDI, under the project nr. 130/2012. This paper is supported by the Sectoral Operational Programme Human Resources Development (SOP HRD), ID134378 financed from the European Social Fund and by the Romanian Government.

References

[1] J.R. Cebral, F. Mut, J. Weir, C.M. Putman, Association of hemodynamic characteristics and cerebral aneurysm rupture, Am. J. Neuroradiol. 32 (2011) 264–270, http://dx.doi.org/10.3174/ajnr.A2274.
[2] C.M. Haggerty, K.R. Kanter, M. Restrepo, D.A. de Zelicourt, W.J. Parks, J. Rossignac, M.A. Fogel, A.P. Yoganathan, Simulating hemodynamics of the Fontan y-graft based on patient-specific in vivo connections, J. Thorac. Cardiovasc. Surg. 145 (2013) 663–670, http://dx.doi.org/10.1016/j.jtcvs.2012.03.076.
[3] A. Quarteroni, M. Tuveri, A. Veneziani, Computational vascular fluid dynamics: problems, models and methods, Comput. Vis. Sci. 2 (2000) 163–197, http://dx.doi.org/10.1007/s007910050039.
[4] C.A. Taylor, D.A. Steinman, Image-based modeling of blood flow and vessel wall dynamics: applications, methods and future directions, Ann. Biomed. Eng. 38 (2010) 1188–1203, http://dx.doi.org/10.1007/s10439-010-9901-0.
[5] N. Westerhof, J.W. Lankhaar, B.E. Westerhof, The arterial windkessel, J. Med. Biol. Eng. 47 (2009) 131–141, http://dx.doi.org/10.1007/s11517-008-0359-2.
[6] M.S. Olufsen, A. Nadim, L.A. Lipsitz, Dynamics of cerebral blood flow regulation explained using a lumped parameter model, Am. J. Physiol. – Reg. I. 282 (2002) 611–622, http://dx.doi.org/10.1152/ajpregu.00285.2001.
[7] R. Spilker, C.A. Taylor, Tuning multidomain hemodynamic simulations to match physiological measurements, Ann. Biomed. Eng. 38 (2010) 2635–2648, http://dx.doi.org/10.1007/s10439-010-0011-9.
[8] M. Ismail, W.A. Wall, M.W. Gee, Adjoint-based inverse analysis of windkessel parameters for patient-specific vascular models, J. Comput. Phys. 244 (2013) 113–130, http://dx.doi.org/10.1016/j.jcp.2012.10.028.
[9] P.J. Blanco, S.M. Watanabe, R.A. Feijo, Identification of vascular territory resistances in one-dimensional hemodynamics simulations, J. Biomech. 45 (2012) 2066–2073, http://dx.doi.org/10.1016/j.jbiomech.2012.06.002.
[10] S. Pant, B. Fabrèges, J.-F. Gerbeau, I.E. Vignon-Clementel, A multiscale filtering-based parameter estimation method for patient-specific coarctation simulations in rest and exercise. Statistical atlases and computational models of the heart, Imaging Model. Challenges 8330 (2014) 102–109, http://dx.doi.org/10.1007/978-3-642-54268-8_12.
[11] P. Moireau, C. Bertoglio, N. Xiao, C.A. Figueroa, C.A. Taylor, D. Chapelle, J.F. Gerbeau, Sequential identification of boundary support parameters in a fluid–structure vascular model using patient image data, Biomech. Model. Mechanobiol. 12 (2013) 475–496, http://dx.doi.org/10.1007/s10237-012-0418-3.
[12] C. Bertoglio, P. Moireau, J.-F. Gerbeau, Sequential parameter estimation for fluid–structure problems: application to hemodynamics, Int. J. Numer. Methods Biomed. Eng. 28 (2012) 434–455, http://dx.doi.org/10.1002/cnm.1476.
[13] P. Reymond, Y. Bohraus, F. Perren, F. Lazeyras, N. Stergiopulos, Validation of a patient-specific one-dimensional model of the systemic arterial tree, Am. J. Physiol., Heart Circ. Physiol. 301 (2011) 1173–1182, http://dx.doi.org/10.1152/ajpheart.00821.2010.
[14] N. Stergiopulos, D.F. Young, T.R. Rogge, Computer simulation of arterial flow with applications to arterial and aortic stenosis, J. Biomech. 25 (1992) 1477–1488, http://dx.doi.org/10.1016/0021-9290(92)90060-E.
[15] M. Olufsen, C. Peskin, W.Y. Kim, E.M. Pedersen, A. Nadim, J. Larsen, Numerical simulation and experimental validation of blood flow in arteries with structured-tree outflow conditions, Ann. Biomed. Eng. 28 (28) (2000) 1281–1299, http://dx.doi.org/10.1114/1.1326031.
[16] L. Formaggia, D. Lamponi, A. Quarteroni, One dimensional models for blood flow in arteries, J. Eng. Math. 47 (2003) 251–276, http://dx.doi.org/10.1023/B:ENGI.0000007980.01347.29.
[17] J.P. Mynard, P. Nithiarasu, A 1D arterial blood flow model incorporating ventricular pressure, aortic valve and regional coronary flow using the locally conservative Galerkin (LCG) method, Commun. Numer. Methods Eng. 24 (24) (2008) 367–417, http://dx.doi.org/10.1002/cnm.1117.
[18] J. Alastruey, A. Khir, K. Matthys, P. Segers, S. Sherwin, P. Verdonck, K. Parker, J. Peiro, Pulse wave propagation in a model human arterial network: assessment of 1-D visco-elastic simulations against in vitro measurements, J. Biomech. 44 (2011) 2250–2258, http://dx.doi.org/10.1016/j.jbiomech.2011.05.041.
[19] C. Malossi, P. Blanco, S. Deparis, A two-level time step technique for the partitioned solution of one-dimensional arterial networks, Comput. Methods Appl. Math. 237 (2012) 212–226, http://dx.doi.org/10.1016/j.cma.2012.05.017.

[20] L. Itu, P. Sharma, V. Mihalef, A. Kamen, C. Suciu, D. Comaniciu, A patient-specific reduced-order model for coronary circulation, in: Proc. of Intern. Symp. on Biomed. Imag., Barcelona, Spain, 2012, pp. 832–835.
[21] R. Raghu, I. Vignon-Clementel, C.A. Figueroa, C.A. Taylor, Comparative study of viscoelastic arterial wall models in nonlinear one-dimensional finite element simulations of blood flow, J. Biomech. Eng. 133 (2011) 081003, http://dx.doi.org/10.1115/1.4004532.
[22] K. Low, R. van Loon, I. Sazonov, R.L.T. Bevan, P. Nithiarasu P, An improved baseline model for a human arterial network to study the impact of aneurysms on pressure-flow waveforms, Int. J. Numer. Methods Biomed. Eng. 28 (2012) 1224–1246, http://dx.doi.org/10.1002/cnm.2533.
[23] L. Itu, P. Sharma, K. Ralovich, V. Mihalef, R. Ionasec, A. Everett A, R. Ringel, A. Kamen, D. Comaniciu, Non-invasive hemodynamic assessment of aortic coarctation: validation with in vivo measurements, Ann. Biomed. Eng. 41 (2013) 669–681, http://dx.doi.org/10.1007/s10439-012-0715-0.
[24] J.P. Mynard, M.R. Davidson, D.J. Penny, J.J. Smolich, A simple, versatile valve model for use in lumped parameter and one-dimensional cardiovascular models, Int. J. Numer. Methods Biomed. Eng. 28 (2012) 626–641, http://dx.doi.org/10.1002/cnm.1466.
[25] J.R. Womersley, Method for the calculation of velocity, rate of flow and viscous drag in arteries when the pressure gradient is known, J. Physiol. 127 (1955) 553–563.
[26] Y. Huo, M. Svendsen, J.S. Choy, Z.D. Zhang, G.S. Kassab, A validated predictive model of coronary fractional flow reserve, J. R. Soc. Interface 9 (2012) 1325–1338, http://dx.doi.org/10.1098/rsif.2011.0605.
[27] D.F. Young, N.R. Cholvin, A.C. Roth, Pressure drop across artificially induced stenoses in the femoral arteries of dogs, Circ. Res. 36 (1975) 735–743.
[28] B.N. Steele, Using one-dimensional finite element analysis to estimate differential pressure of renal artery stenoses, in: Proc. of Comp. in Cardiology, Durham, NC, USA, 2007, pp. 381–384.
[29] D. Bessems, On the propagation of pressure and flow waves through the patient-specific arterial system, PhD Thesis, TU Eindhoven, Netherlands, 2007.
[30] M. Zamir, P. Sinclair, T.H. Wonnacott, Relation between diameter and flow in major branches of the arch of the aorta, J. Biomech. 25 (1992) 1303–1310, http://dx.doi.org/10.1016/0021-9290(92)90285-9.
[31] C.D. Murray, The physiological principle of minimum work: I. the vascular system and the cost of blood volume, Proc. Natl. Acad. Sci. USA 12 (1926) 207–214.
[32] L. Grinberg, G.E. Karniadakis, Outflow boundary conditions for arterial networks with multiple outlets, Ann. Biomed. Eng. 36 (2008) 1496–1514, http://dx.doi.org/10.1007/s10439-008-9527-7.
[33] N. Stergiopulos, J.J. Meister, N. Westerhof, Simple and accurate way for estimating total and segmental arterial compliance: the pulse pressure method, Ann. Biomed. Eng. 22 (1994) 392–397, http://dx.doi.org/10.1007/BF02368245.
[34] Z. Keshavarz-Motamed, J. Garcia, P. Pibarot, E. Larose, L. Kadem, Modeling the impact of concomitant aortic stenosis and coarctation of the aorta on left ventricular workload, J. Biomech. 44 (2011) 2817–2825, http://dx.doi.org/10.1016/j.jbiomech.2011.08.00.
[35] J.F.J. LaDisa, C.A. Figueroa, I.E. Vignon-Clementel, H.J. Kim, N. Xiao, L.M. Ellwein, F.P. Chan, J.A. Feinstein, C.A. Taylor, Computational simulations for aortic coarctation: representative results from a sampling of patients, J. Biomech. Eng. 133 (2011) 091008, http://dx.doi.org/10.1115/1.4004996.
[36] M. Ismail, M.W. Gee, W.A. Wall, CFD challenge: hemodynamic simulation of a patient-specific aortic coarctation model with adjoint-based calibrated windkessel elements, Lect. Notes Comput. Sci. 7746 (2013) 44–52, http://dx.doi.org/10.1007/978-3-642-36961-2_6.
[37] M. Ismail, M.W. Gee, W.A. Wall, CFD challenge: simulation of hemodynamics in a patient-specific aortic coarctation model, http://www.vascularmodel.org/miccai2012/, accessed 15/06/2013.
[38] M. Ismail, M.W. Gee, W.A. Wall, The vascular modeling toolkit, http://www.vmtk.org/, accessed 01/05/2014.
[39] B.N. Steele, J. Wan, J.P. Ku, T.J.R. Hughes, C.A. Taylor, In vivo validation of a one-dimensional finite-element method for predicting blood flow in cardiovascular bypass grafts, IEEE Trans. Biomed. Eng. 50 (2003) 649–656, http://dx.doi.org/10.1109/TBME.2003.812201.